Nonuniformity of Chain-Length Distributions in Photopolymerized Layers

Guillermo Terrones*

Applied Physics Division, Los Alamos National Laboratory, Los Alamos, New Mexico 87545

Arne J. Pearlstein*

Department of Mechanical and Industrial Engineering, University of Illinois at Urbana−Champaign, 1206 West Green Street, Urbana, Illinois 61801

Received October 14, 2002; Revised Manuscript Received May 28, 2003

ABSTRACT: For free-radical photopolymerization with a photobleaching initiator, constant chain propagation and termination rate constants k_p and k_t, and termination occurring only by recombination, we account for Beer−Lambert attenuation and initiator consumption to predict how spatial variation of the final chain length distribution (CLD) depends on k_p, k_t, incident light intensity I_o, layer thickness L, photoinitiator absorption coefficient α_A and initial concentration $C_{A,0}$, and quantum yield of photoinitiator consumption ϕ, for a typical value (10^{-4}) of the initial ratio of initiator and monomer concentrations $C_{A,0}/C_{M,0}$. We show how spatial variation of the final CLD depends on initial absorbance $\gamma = \alpha_A C_{A,0} L$ and a parameter $\beta = k_p[fC_{A,0}/(\phi\alpha_A I_o k_t)]^{1/2}$, where f primary radicals are produced per photoinitiator molecule consumed. For small γ, the number-averaged mean chain length increases with depth at each β and with β at each depth. The chain length at which the CLD achieves its maximum value, along with a measure of polydispersity (half the CLD width at half-maximum, divided by the number-averaged mean), increase with depth at small β and decrease with depth at large β, with the CLD having its minimum nonuniformity at intermediate β. Front-to-rear CLD variation increases as γ increases. At small β, nonuniformity is confined to a progressively smaller portion of the front of the layer as γ increases, while for large β, spatial variation is more evenly distributed. The results are discussed in terms of spatiotemporal variation of initiation and monomer conversion. Examples from the literature are used to illustrate the degree of CLD nonuniformity that can be expected in experiments.

Introduction

Understanding the dependence of molecular weight or chain length distributions on reaction conditions in photopolymerizations is important in predicting the relationship between processing parameters (e.g., photoinitiator concentration, incident light intensity, reaction time, layer thickness) and material properties.

Photoinitiation in strongly absorbing or thick layers can be highly nonuniform and lead to highly nonuniform monomer conversion rates, as recognized long ago.[1] We recently considered the effects of optical attenuation and photoinitiator consumption on spatiotemporal variation of initiation[2] and monomer conversion[3] rates in systems with photobleaching initiators. In that work, we discussed studies of the sensitivity of material properties and performance to spatial variation of monomer conversion, cross-linking, and other sources of heterogeneity (e.g., pools of unreacted monomer), as well as previous work on nonuniformity in photopolymerizations, especially at high initial absorbance (e.g., high initiator concentration or deep layers). We also presented detailed results on the spatiotemporal variation of the concentration of a photobleaching initiator, the photoinitiation rate, and the completeness, uniformity, and rate of monomer conversion in free-radical photopolymerizations in such systems. Here, we focus on predicting the chain length distribution (CLD) and its variation with depth in a layer of photopolymerized material.

As discussed earlier,[2,3] standard treatments of free-radical photopolymerization kinetics ignore spatiotemporal variation of initiator or monomer concentrations. Recent computational simulations of photopolymerization in specific monomer/initiator systems, including simulations accounting for spatial variation of monomer conversion,[4,5] have not predicted CLDs. Studies of spatial variation of properties in photopolymerized materials have been limited to nonuniform monomer conversion (primarily "depth of cure"[6]), primarily in dental applications.[7−12] Nonuniformity is important in localizing photopolymerization to thin layers in three-dimensional structures fabricated by microstereophotolithography,[13−16] and might also play a role in "undercutting" in postexposure wash-off in proofing and printing applications involving photopolymers and contribute to difficulties in layer separation of multilayered photopolymer films.

Our previous work[2,3] suggests that at high initial absorbance, nonuniform photoinitiation rates and monomer conversion will give rise to nonuniform CLDs. The only related work of which we are aware is the experimental study of Mateo et al.,[19] who showed how the intrinsic viscosity of poly(methyl acrylate) increased with decreasing concentration of a photobleaching initiator. Those authors pointed out that at high initial absorbances, light absorption is localized near the optical entrance, leading to high concentrations and termination rates of primary radicals, and lower molecular weights there. Like other quantities, spatial variation of the CLD and its moments cannot be predicted by kinetic models that ignore nonuniform photoinitiator consumption and monomer conversion. While nonuniform monomer conversion in photopolymerization experiments has been reported,[20] we are aware of no reports of spatial variation of CLDs.

* To whom correspondence should be directed.

10.1021/ma021589k CCC: $25.00
Published on Web 08/01/2003

Table 1. List of Notation

symbol	quantity	definition	units
C_j	concentration of species j		M
$C_{j,0}$	initial concentration of species j		M
f	no. of primary radicals created per photoinitiator molecule consumed		
I	light intensity		einsteins $m^{-2}\,s^{-1}$
I_o	incident light intensity		einsteins $m^{-2}\,s^{-1}$
k_p	propagation rate constant		$M^{-1}\,s^{-1}$
k_t	termination rate constant	$k_{t,m,n}$ $(m \neq n)$	$M^{-1}\,s^{-1}$
$k_{t,m,n}$	termination rate constant for reaction of $RM_m^\bullet$ and $RM_n^\bullet$		$M^{-1}\,s^{-1}$
L	layer depth		m
M_j	molecular mass of species j		g mol^{-1}
$\overline{M}_n$	no.-averaged molecular mass		g mol^{-1}
$\overline{M}_w$	mass-averaged molecular mass		g mol^{-1}
R_{init}	initiation rate		M s^{-1}
S_j	dimensionless concentration of species j	$C_j/C_{j,0}$	
w_j	mole fraction of species j	eq 19	
x	dimensional coordinate		m
X_{max}	chain length at which w is maximum		
$\overline{X}_n$	no.-averaged mean chain length		
z	dimensionless coordinate	x/L	
α_A	absorption coeff of photoinitiator		$M^{-1}\,m^{-1}$
β	dimensionless "kinetic" parameter	$k_p[f C_{A,0}/\phi\alpha_A I_o k_t)]^{1/2}$	
Γ	measure of polydispersity		
γ	initial absorbance	$\alpha_A C_{A,0} L$	
ϵ_A	extinction coeff of photoinitiator		$M^{-1}\,m^{-1}$
θ	right-hand side of eq 24		
σ	$k_t\theta/(k_p S_M)$		
τ	dimensionless time	$\phi I_o \alpha_A t$	
ϕ	quantum yield of initiator consumption		
ζ	ratio of initial photoinitiator concentration to initial monomer concentration		

Here, we use our earlier results on nonuniform photoinitiation and monomer conversion[2,3] as a foundation to study how spatial variation of the CLD depends on initial photoinitiator and monomer concentrations, light intensity, propagation and termination rate constants, layer depth, photoinitiator absorption coefficient, and quantum yield of photoinitiator consumption. We employ a standard kinetic model, with propagation and termination rate constants independent of the degree of conversion. We discuss mechanistic sources of uncertainty, cessation of illumination before complete exhaustion of initiator, and implications for experiments. Beyond insight into systems of practical interest, the calculations provide a benchmark to which results for more complex kinetics (e.g., accounting for autoacceleration or autodeceleration) can be compared.

Model

We consider the same mechanism[21,22] discussed in our earlier work on the completeness and uniformity of monomer conversion,[3] viz.

$$A \xrightarrow{h\nu} f R^\bullet \tag{1}$$

$$R^\bullet + M \xrightarrow{k_p} RM^\bullet \tag{2}$$

$$RM_i^\bullet + M \xrightarrow{k_p} RM_{i+1}^\bullet \quad i \geq 1 \tag{3}$$

$$RM_i^\bullet + RM_j^\bullet \xrightarrow{k_{t,i,j}} RM_{i+j}R \quad i,j \geq 0 \tag{4}$$

in which all light absorption is by the photoinitiator A, whose photolysis leads to f primary radicals $R^\bullet$. We take the chain initiation and propagation reactions, eqs 2 and 3, to have the same rate constant k_p, which together with the termination rate constants $k_{t,i,j}$, is independent of chain length and degree of conversion of the monomer, M. We assume that termination occurs solely by recombination, (4), with no disproportionation. The factor f accounts for the possibilities that initiator photolysis can lead to one or two primary radicals, or that some primary radicals neither initiate chains nor recombine with a radical chain or another primary radical.

Neglecting diffusion[23] and convection[24,25] which sometimes occur in photopolymerizations, we obtain the kinetic equations

$$\frac{\partial C_A}{\partial t} = -\phi\alpha_A I(x,t) C_A \tag{5a}$$

$$\frac{\partial C_{R\bullet}}{\partial t} = f\phi\alpha_A I(x,t) C_A - k_p C_M C_{R\bullet} - 2k_{t,0,0} C_{R\bullet}^2 - \sum_{j=1}^{\infty} k_{t,0,j} C_{R\bullet} C_{RM_j\bullet} \tag{5b}$$

$$\frac{\partial C_{RM_i\bullet}}{\partial t} = k_p C_M [C_{RM_{i-1}\bullet} - C_{RM_i\bullet}] - C_{RM_i\bullet} \sum_{\substack{j=0 \\ j\neq i}} k_{t,i,j} C_{RM_j\bullet} - 2k_{t,i,i} C_{RM_i\bullet}^2 \quad i \geq 1 \tag{5c}$$

$$\frac{\partial C_M}{\partial t} = -k_p C_M \sum_{j=0}^{\infty} C_{RM_j\bullet} \tag{5d}$$

$$\frac{\partial C_{RM_iR}}{\partial t} = \sum_{j=0}^{[i/2]} k_{t,j,i-j} C_{RM_j\bullet} C_{RM_{i-j}\bullet} \quad i \geq 0 \tag{5e}$$

where $[i/2]$ is the largest integer not exceeding $i/2$, and $C_{RM_0\bullet}$ and $C_{R\bullet}$ both represent the primary radical concentration. Defining $k_t = k_{t,i,j}$ for $i \neq j$, we take $k_{t,i,i} = k_t/2$, as discussed in standard texts,[21,22] and note from (4) that $k_{t,i,j} = k_{t,j,i}$. Here, α_A is the absorption coefficient[26] of the initiator, C_l is the molar concentration of species l, and the dependence of the light intensity $I(x,t)$ on position and time is explicitly indicated. A list of notation is provided in Table 1. We neglect any dependence of k_p, k_t, and α_A on temperature, equivalent

to assuming that the process is isothermal or that these three parameters are insensitive to temperature variation.

As in our earlier work,[2,3] we assume that light absorption can be modeled with a single value of α_A in (5a), corresponding to monochromatic irradiation or to α_A being constant over the range of actinic wavelengths. We consider a layer of thickness L illuminated normal to the $z = 0$ surface and assume that the moieties resulting from initiator photolysis are transparent at the actinic wavelength(s). Photobleaching initiators are particularly attractive, as they can provide high local initiation rates as a "front" propagates through the layer in the direction of the incident beam,[2] allowing thick sections (up to several centimeters) to be cured rapidly.[20,28,29] We assume that Beer's law

$$I(x,t) = I_o \exp[-\alpha_A \int_0^x C_A(x',t)\, dx'] \tag{6}$$

describes the variation of light intensity along the beam path, from its incident value I_o at the optical entrance. Limitations of this model are considered in the Discussion.

We assume that at $t = 0$, initiator and monomer concentrations are uniform throughout the layer, and no other species are present. Thus

$$C_A(x,0) = C_{A,0} \tag{7a}$$

$$C_M(x,0) = C_{M,0} \tag{7b}$$

Summing (5b) and (5c) and making the usual steady-state approximation for the total radical concentration,[1,3,21,22] which is reasonable if the radical lifetimes are small compared to the time scales for initiator consumption and monomer conversion, we obtain the total radical concentration

$$\sum_{j=0}^{\infty} C_{RM_j^\cdot} = \sqrt{f\phi\alpha_A I(x,t) C_A / k_t} \tag{8}$$

from which it follows that

$$\frac{\partial C_M}{\partial t} = -k_p \sqrt{f\phi\alpha_A I(x,t) C_A / k_t}\, C_M \tag{9}$$

Thus, within the limitations of the steady-state approximation on the radical concentrations, local conversion of monomer can be determined by solving (5a) and (9), subject to the initial conditions (7a,b). Since monomer is consumed by (2) and (3), derivation of (9) requires that the summation in (8) begin with $j = 0$ (the primary radical concentration).

To nondimensionalize these equations, we introduce a dimensionless time $\tau = \phi I_o \alpha_A t$, position $z = x/L$, concentrations $S_l = C_l/C_{l,0}$ (l = A,M), and initial absorbance $\gamma = \alpha_A C_{A,0} L$. As shown earlier, the dimensionless initiator concentration is given in terms of these variables by[2]

$$S_A = [1 + e^{-\gamma z}(e^{\tau} - 1)]^{-1} \tag{10}$$

while the dimensional rate of formation of primary radicals is given by

$$R_{init} = f\phi\alpha_A I C_A = \frac{f\phi\alpha_A I_0 e^{\tau-\gamma z} C_{A,0}}{[1 + e^{-\gamma z}(e^{\tau} - 1)]^2} \tag{11}$$

where the light intensity can be written as

$$I = \frac{I_o e^{\tau-\gamma z}}{1 + e^{-\gamma z}(e^{\tau} - 1)} \tag{12}$$

The local total radical concentration given by (8) is proportional to the square root of the initiation rate given by (11), whose variation (e.g., traveling-wave behavior at large initial absorbances) was discussed earlier.[2]

The kinetic equation (eq 9) for monomer concentration can be written in dimensionless form as

$$\frac{\partial S_M}{\partial \tau} = -\beta \frac{e^{(\tau-\gamma z)/2}}{1 + e^{-\gamma z}(e^{\tau} - 1)} S_M \tag{13}$$

subject to the initial condition

$$S_M(z,0) = 1 \tag{14}$$

where

$$\beta = k_p \left[\frac{f C_{A,0}}{\phi\alpha_A I_o k_t}\right]^{1/2} \tag{15}$$

is seen from eqs 5a and 9 to be the first-order rate constant for monomer conversion divided by the first-order rate constant for photoinitiator consumption, both evaluated at $z = \tau = 0$.

Analysis

The variation of monomer conversion can be found from solution of (13) subject to the initial condition given by (14). Since γ and β depend on $C_{A,0}$ and α_A, but only β depends on k_p, k_t, and I_o, it will prove useful to think of β as a kinetic parameter. The solution of (13) and (14) is given by[3]

$$S_M(z,\tau) = \exp\left\{-\frac{2\beta}{(1 - e^{-\gamma z})^{1/2}} \arctan\left[\frac{(e^{\gamma z} - 1)^{1/2}(e^{\tau/2} - 1)}{e^{\gamma z} - 1 + e^{\tau/2}}\right]\right\} \tag{16}$$

as can be verified by substitution.

The dimensionless instantaneous local concentration of "dead" polymer RM_iR is defined by

$$S_{RM_iR}(z,\tau) = C_{RM_iR}(z,\tau)/C_{M,0}, \quad i \geq 0 \tag{17}$$

which can be written as

$$S_{RM_iR}(z,\tau) = \frac{C_{M,0}}{\phi I_o \alpha_A} \int_0^{\tau} \sum_{j=0}^{[i/2]} k_{t,j,i-j} S_{RM_j^\cdot}(z,\tau') S_{RM_{i-j}^\cdot}(z,\tau')\, d\tau', \quad i \geq 0 \tag{18}$$

upon integration of (5e). The mole fractions of dead chains can be defined by

$$w_{\mathrm{RM}_i\mathrm{R}}(z,\tau) = \frac{S_{\mathrm{RM}_i\mathrm{R}}(z,\tau)}{S_{\mathrm{M}}(z,\tau) + \sum_{j=0}^{\infty} S_{\mathrm{RM}_j\mathrm{R}}(z,\tau)}, \quad i \geq 0 \quad (19)$$

in which we neglect primary and chain radical concentrations in the denominator. This is an excellent approximation, except possibly when the number of moles of stable species is very small (e.g., when nearly all monomer at a given z has been converted into a small number of long polymer molecules), and the number of radicals is significant. (This is not an issue in the results presented below, which pertain to the final state, for which radical concentrations are zero.) We note that $w_{\mathrm{RM}_i\mathrm{R}}$ is defined as the number of moles of dead polymer with chain length i, divided by the number of moles of all stable species present, including any unreacted monomer.

In terms of mole fractions, the number- and weight-averaged molecular weights are defined by

$$\overline{M}_{\mathrm{n}}(z,\tau) = \frac{\sum_{j=0}^{\infty}(jM_{\mathrm{M}} + 2M_{\mathrm{R}})w_{\mathrm{RM}_j\mathrm{R}}(z,\tau)}{w_{\mathrm{M}}(z,\tau) + \sum_{j=0}^{\infty} w_{\mathrm{RM}_j\mathrm{R}}(z,\tau)} \quad (20a)$$

and

$$\overline{M}_{\mathrm{w}}(z,\tau) = \frac{\sum_{j=0}^{\infty}(jM_{\mathrm{M}} + 2M_{\mathrm{R}})^2 w_{\mathrm{RM}_j\mathrm{R}}(z,\tau)}{M_{\mathrm{M}} w_{\mathrm{M}}(z,\tau) + \sum_{j=0}^{\infty}(jM_{\mathrm{M}} + 2M_{\mathrm{R}})w_{\mathrm{RM}_j\mathrm{R}}(z,\tau)} \quad (20b)$$

respectively, where M_{M} and M_{R} are the formula masses of the monomer and primary radical moieties in polymerized material, and

$$w_{\mathrm{M}}(z,\tau) = \frac{S_{\mathrm{M}}(z,\tau)}{S_{\mathrm{M}}(z,\tau) + \sum_{j=0}^{\infty} S_{\mathrm{RM}_j\mathrm{R}}(z,\tau)} \quad (21)$$

In what follows, we will use the number-averaged chain length

$$\overline{X}_{\mathrm{n}}(z,\tau) = \frac{\sum_{j=0}^{\infty} j w_{\mathrm{RM}_j\mathrm{R}}(z,\tau)}{\sum_{j=0}^{\infty} w_{\mathrm{RM}_j\mathrm{R}}(z,\tau)} \quad (22)$$

which allows us to present results for general values of M_{M} and M_{R}. Note that since the denominator in (19) is independent of the chain length index, $\overline{X}_{\mathrm{n}}$ will be independent of the unreacted monomer mole fraction w_{M}, even though the mole fractions $w_{\mathrm{RM}_i\mathrm{R}}$ depend on w_{M}.

Making the steady-state approximation for each i in (5c) and introducing the dimensionless variables defined above, we find

$$\frac{S_{\mathrm{RM}_{i-1}\cdot}}{S_{\mathrm{RM}_i\cdot}} = 1 + \frac{k_{\mathrm{t}}}{k_{\mathrm{p}} S_{\mathrm{M}}} \sum_{j=0}^{\infty} S_{\mathrm{RM}_j\cdot}, \quad i \geq 1 \quad (23)$$

Summing (5c) over i, adding (5b), making the steady-state approximation for the total radical concentration, and nondimensionalizing radical concentrations by dividing by $C_{\mathrm{M},0}$, we obtain

$$\sum_{j=0}^{\infty} S_{\mathrm{RM}_j\cdot} = \sqrt{f\phi\alpha_{\mathrm{A}}\zeta I_{\mathrm{o}}/(k_{\mathrm{t}} C_{\mathrm{M},0})}\, \mathrm{e}^{(\tau-\gamma z)/2} S_{\mathrm{A}}(z,\tau) \quad (24)$$

where $\zeta = C_{\mathrm{A},0}/C_{\mathrm{M},0}$ and we have used (10). Defining θ as the right-hand side of (24), we obtain

$$S_{\mathrm{RM}_i\cdot} = \frac{S_{\mathrm{RM}_{i-1}\cdot}}{1 + k_{\mathrm{t}}\theta/(k_{\mathrm{p}} S_{\mathrm{M}})}, \quad i \geq 1 \quad (25)$$

from (23). Summing (5c) over the index, we get

$$S_{\mathrm{R}\cdot} = \frac{k_{\mathrm{t}}\theta^2}{k_{\mathrm{p}} S_{\mathrm{M}} + k_{\mathrm{t}}\theta} \quad (26)$$

from which we find that

$$S_{\mathrm{RM}_i\cdot} = \frac{\sigma\theta}{(1+\sigma)^{i+1}}, \quad i \geq 0 \quad (27)$$

where $\sigma(z,\tau) = k_{\mathrm{t}}\theta/(k_{\mathrm{p}} S_{\mathrm{M}})$. From (18), it follows that

$$S_{\mathrm{RM}_i\mathrm{R}}(z,\tau) = \frac{C_{\mathrm{M},0}}{\phi I_{\mathrm{o}}\alpha_{\mathrm{A}}} \int_0^{\tau} \sum_{j=0}^{[i/2]} k_{\mathrm{t},\,j,i-j} \frac{\sigma^2(z,\tau')\theta^2(z,\tau')}{[1+\sigma(z,\tau')]^{i+2}}\, \mathrm{d}\tau', \quad i \geq 0 \quad (28a)$$

$$= \frac{(i+1)C_{\mathrm{M},0}k_{\mathrm{t}}}{2\phi I_{\mathrm{o}}\alpha_{\mathrm{A}}} \int_0^{\tau} \frac{\sigma^2(z,\tau')\theta^2(z,\tau')}{[1+\sigma(z,\tau')]^{i+2}}\, \mathrm{d}\tau', \quad i \geq 0 \quad (28b)$$

so that the summation in the denominator of (19) can be written as

$$\sum_{j=0}^{\infty} S_{\mathrm{RM}_j\mathrm{R}}(z,\tau) = \frac{C_{\mathrm{M},0}k_{\mathrm{t}}}{2\phi I_{\mathrm{o}}\alpha_{\mathrm{A}}} \int_0^{\tau} \sigma^2(z,\tau')\theta^2(z,\tau') \times \sum_{j=0}^{\infty} \frac{j+1}{[1+\sigma(z,\tau')]^{j+2}}\, \mathrm{d}\tau' \quad (29a)$$

$$= \frac{C_{\mathrm{M},0}k_{\mathrm{t}}}{2\phi I_{\mathrm{o}}\alpha_{\mathrm{A}}} \int_0^{\tau} \theta^2(z,\tau')\, \mathrm{d}\tau' = \frac{f\zeta}{2}[1 - S_{\mathrm{A}}(z,\tau)] \quad (29b)$$

where we have again used (10).

Using (29b), we can now rewrite the mole fractions (19) as

$$w_{\mathrm{RM}_i\mathrm{R}}(z,\tau) = \frac{\frac{C_{\mathrm{M},0}k_{\mathrm{t}}(i+1)}{2\phi I_{\mathrm{o}}\alpha_{\mathrm{A}}} \int_0^{\tau} \frac{\sigma^2(z,\tau')\theta^2(z,\tau')}{[1+\sigma(z,\tau')]^{i+2}}\, \mathrm{d}\tau'}{S_{\mathrm{M}}(z,\tau) + \frac{f\zeta}{2}[1 - S_{\mathrm{A}}(z,\tau)]}, \quad i \geq 1 \quad (30)$$

After some analysis, it can be shown that the number-averaged chain length is

$$\overline{X}_n(z,\tau) = \frac{2[1 + (e^{\gamma z} - 1)e^{-\tau}]}{f\zeta(1 - e^{-\tau})}\left[1 - \exp\left\{\frac{-2\beta \arctan[(e^{\gamma z} - 1)^{1/2}(e^{\tau/2} - 1)/(e^{\tau/2} + e^{\gamma z} - 1)]}{(1 - e^{-\gamma z})^{1/2}}\right\}\right] \quad (31)$$

from which it follows that the final number-averaged chain length (i.e., when all initiator has been consumed and monomer conversion has ended) is

$$\overline{X}_n(z,\infty) = \frac{2}{f\zeta}\left[1 - \exp\left\{\frac{-2\beta \arctan[(e^{\gamma z} - 1)^{1/2}]}{(1 - e^{-\gamma z})^{1/2}}\right\}\right] \quad (32)$$

It can be shown that the weight-averaged chain length grows without bound as monomer is completely converted. This divergence is not unique to our model and has been noted for other polymerization models and CLDs since the work of Flory,[30] where for the "most probable" distribution, the number-averaged molecular weight is well-behaved at all conversions, while the weight-averaged molecular weight diverges as monomer is completely converted.

As $\beta \to 0$, the final number-averaged chain length vanishes asymptotically like

$$\overline{X}_n(z,\infty) \sim \frac{4\beta}{f\zeta}\frac{\arctan[(e^{\gamma z} - 1)^{1/2}]}{(1 - e^{-\gamma z})^{1/2}} \quad (33)$$

We also see from (32) that $\overline{X}_n(z,\infty)$ has the small-γ Taylor series expansion

$$\overline{X}_n(z,\infty) = \frac{2}{f\zeta}\left\{1 - e^{-2\beta}\left[1 - \frac{\beta\gamma z}{3} + O(\gamma^2 z^2)\right]\right\} \quad (34)$$

from which it follows that $\overline{X}_n(z,\infty)$ approaches a z-independent constant as $\gamma \to 0$. For a particular initiator with a given α_A, this is the appropriate limit as either the initial initiator concentration $C_{A,0}$ or layer thickness L vanishes. We also note that

$$\lim_{z \to 0} \overline{X}_n(z,\infty) = \lim_{\gamma \to 0} \overline{X}_n(z,\infty) = \frac{2(1 - e^{-2\beta})}{f\zeta} \quad (35)$$

and

$$\lim_{\gamma z \to \infty} \overline{X}_n(z,\infty) = \frac{2(1 - e^{-\beta\tau})}{f\zeta} \quad (36)$$

Finally, we define a local polydispersity measure $\Gamma(z)$ as half the width of the final CLD at half of its maximum value, divided by $\overline{X}_n(z,\infty)$. Unlike the usual "polydispersity index," Γ is well-defined even when the mass-averaged chain length is unbounded. It also varies continuously with the final CLD, including when the maximum of the final CLD moves to zero chain length.

Results

For a range of γ and β and the typical value $\zeta = C_{A,0}/C_{M,0} = 10^{-4}$, the final mole fractions w_{RM_iR} were obtained by evaluating (30) as $\tau \to \infty$, with the range of temporal integration being transformed to a finite one by a logarithmic change of variable. Gauss−Kronrod adaptive quadrature with error estimation at the Kronrod points was used, with sufficient quadrature points to make the magnitude of the relative error less than 10^{-6}. In what follows, references to CLDs, mole fractions, and monomer conversion pertain to the final state unless otherwise indicated.

We organize the results according to the initial absorbance γ, the dominant parameter in determining CLD nonuniformity. For $\gamma = 1$ and 10, and several values of the kinetic parameter β between 0.05 and 100, we show $\overline{X}_n(z,\infty)$, $X_{max}(z,\infty)$ (the chain length for which the mole fraction is largest at each z), and the polydispersity measure $\Gamma(z)$. At each γ, these results are followed by presentation of final CLDs as functions of chain length k at six uniformly distributed values of z. The values of γ cover the range in which light intensity is initially reduced to 1/e of its incident value at $x = L$ and $0.1L$ (or equivalently to 1/e and e^{-10}, respectively, at $x = L$) and provide insight into the entire range of initial absorbances. The range of β covers behavior from very small to very large ratios of the rates of polymerization and initiation. The ranges of γ and β considered encompass values pertinent to the experiments considered in the Discussion.

$\gamma = 1$. For $\gamma = 1$ and a range of β, Figure 1a shows that $\overline{X}_n$ increases monotonically with z and β, approaching a uniform (z-independent) limit as $\beta \to \infty$. For $f = 2$, the limit is $1/\zeta$, as seen from (32). As β decreases, the layer-averaged degree of monomer conversion decreases, and conversion at $z = 1$ relative to $z = 0$ increases. As discussed earlier,[3] the latter effect is due to the fact that monomer conversion occurs at lower radical concentrations downbeam than near the optical entrance, which leads to longer chain lengths due to slower net recombination. When β is small, not all monomer is converted, with more remaining at $z = 0$ than at $z = 1$. This leads to the spatial variation in $\overline{X}_n(z,\infty)$ shown in Figure 1a, and to the predicted dependence on β. The approximately linear dependence of $\overline{X}_n(0,\infty)$ on β at small β is consistent with (33). Aside from slight curvature at intermediate β, the $\gamma = 1$ results agree well with the low-absorbance limit (34).

Figure 1b shows that X_{max} increases with z at small β, and that its z variation follows that of $\overline{X}_n$. Monomer conversion also increases with z due to downbeam conversion at low radical concentrations.[3] (As shown in Figure 2a of ref 3, monomer conversion for $\gamma = 1$ and $\beta = 0.1$ increases from 18% at $z = 0$ to 20% at $z = 1$.) As β increases, so does $X_{max}(z,\infty)$. At $\beta = 0.6018$, we have $dX_{max}/dz = 0$ at $z = 1$. For $0.6018 < \beta < 1.0207$, the largest X_{max} occurs in the interior of the layer, and moves toward $z = 0$ as β increases. For $\beta > 1.0207$, X_{max} decreases with z at each β, and with β at each z. The large-β results are understood by noting that at sufficiently high β, monomer conversion downbeam of the propagating front occurs at very low radical concentrations, leading to most of the monomer being incorporated into a small number of long chains before most of the initiator has been consumed. Continued illumination leads to initiator being consumed under conditions where little monomer remains. In that case, primary radicals and radical chains recombine at increasingly short chain lengths, leading to a large number of very short dead chains. These effects are strongest at the rear of the layer, where radical concentrations are lowest and initiator consumption occurs later than farther upbeam.

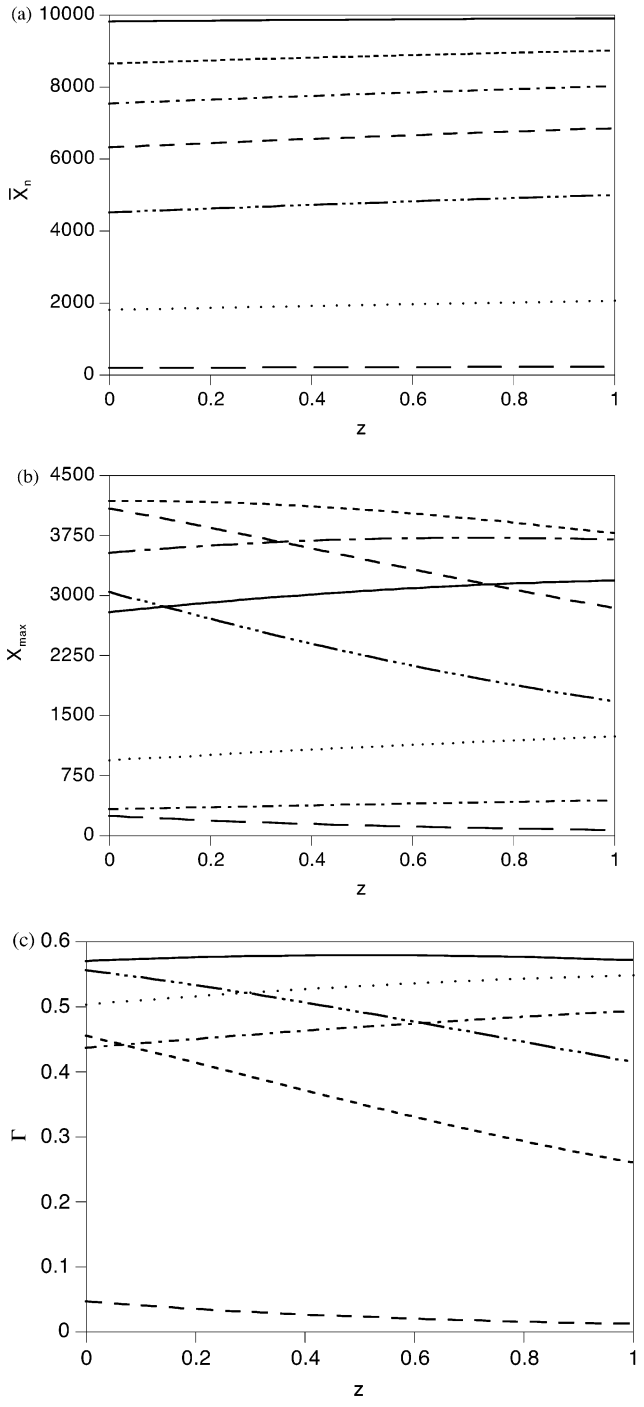

Figure 1. Spatial variation of $\bar{X}_n(z,\infty)$, $X_{max}(z,\infty)$, and $\Gamma(z)$ for $\gamma = 1$ and $\zeta = 10^{-4}$ for selected values of β. (a) $\bar{X}_n(z,\infty)$: (— —) $\beta = 0.01$; (···) $\beta = 0.1$; (— ··· —) $\beta = 0.3$; (— —) $\beta = 0.5$; (— · — · —) $\beta = 0.7$; (- -) $\beta = 1$; (—) $\beta = 2$. (b) $X_{max}(z,\infty)$: (— · — · —) $\beta = 0.05$; (···) $\beta = 0.15$; (—) $\beta = 0.5$; (— - —) $\beta = 0.7$; (- -) $\beta = 1$; (— —) $\beta = 1.5$; (— ··· —) $\beta = 2$; (— —) $\beta = 4$. (c) $\Gamma(z)$: (— · — · —) $\beta = 0.01$; (···) $\beta = 0.3$; (—) $\beta = 0.7$; (— ··· —) $\beta = 1.5$; (- -) $\beta = 2$; (— —) $\beta = 4$.

As shown in Figure 1b, this leads at each z to reduction of X_{max} as β increases, with an increasing fraction of monomer being incorporated into a decreasing number of long-chain polymer molecules. Thus, at each z we see that $X_{max} \to 0$ as $\beta \to \infty$, and also as $\beta \to 0$.

Figure 1c shows that Γ, our measure of polydispersity, increases slowly with z for small β, varying by only about 10% over the layer for $\beta = 0.01$. As β increases, so does Γ, whose dependence on z becomes even weaker. For $\beta = 0.7$, Γ is essentially uniform, varying by less than 2% over the layer. For larger β, Γ ultimately decreases and becomes a monotonically decreasing function of z, with the degree of nonuniformity increasing as β increases. The maximum degree of polydispersity corresponds to a situation in which Γ is essentially uniform over the thickness of the layer. The rapid decrease of Γ with increasing β is due to the rapid shift of the final CLD to small k as β increases, as shown below. As indicated by the high-β results in Figure 1c, the width of the CLD decreases more rapidly with β than does $\bar{X}_n(z,\infty)$.

For $\gamma = 1$, Figure 2a–g shows the predicted CLDs over a range of β, in each case at six uniformly spaced z-locations from the front of the layer ($z = 0$) to the rear ($z = 1$). For $\beta = 0.05$, Figure 2a shows that the CLD and X_{max} shift to larger chain lengths k and smaller mole fractions, respectively, as one moves from the front to the rear. The value of k at the maximum, as well as the value of $w_{RM_kR}(z,\infty)$ there, vary nearly linearly with z. We also note that the mole fraction is nearly independent of z near $k = 670$, decreasing with z at smaller k and increasing with z at larger k. Mole fractions vanish at high k for every z.

Figure 2b shows that if β is doubled to 0.1, the CLDs shift to larger k (note the different scale for the ordinate, compared to Figure 2a), as does the chain length at which $w_{RM_kR}(z,\infty)$ is nearly independent of z. The dependence of the CLDs on k is nearly "self-similar," with $2w_{RM_{2k}R}(z,\infty;\beta = 0.1) \approx w_{RM_kR}(z,\infty;\beta = 0.05)$ being an excellent approximation at each z to the relationship between the two CLDs. The overall increase in dead polymer mole fractions at all but the smallest chain lengths can be associated with increased conversion of monomer as β increases, while the shift to larger k can be associated with the larger ratio of the polymerization rate to the initiation rate at larger β.

For $\beta = 0.5$, Figure 2c shows that the CLDs depend less strongly on z than at smaller β. This is attributable to the much higher (and somewhat more uniform) degree of monomer conversion, compared to the $\beta = 0.1$ case.[3] Unlike the CLDs for smaller β, there is no range of k for which $w_{RM_kR}(z,\infty)$ decreases with increasing z. Rather, $w_{RM_kR}(z,\infty)$ is nearly independent of z for $k <$ 2600, and increases monotonically with z for $k >$ 2600.

For $\beta = 1$, Figure 2d shows that $w_{RM_kR}(z,\infty)$ increases with z at all k, and that at small k (less than $X_{max}(z,\infty)$) the dependence on z is considerably stronger than for $\beta = 0.5$. Consistent with Figure 1b, X_{max} is nearly independent of z for $\beta = 1$. Comparison to Figure 3a of ref 3 shows that although monomer conversion for $\beta = 1$ is only slightly nonuniform (varying between 86% and 91% through the layer), the mole fractions of dead polymer are significantly nonuniform, varying by more than 35% near $X_{max}(z,\infty)$ and by much more at large k.

As β increases to 2, Figure 2e shows that the CLDs have become much more nonuniform, and have shifted to smaller k, relative to the $\beta = 1$ case. As presaged by the $\beta = 1$ results, X_{max} now *decreases* with increasing z. We see that $w_{RM_kR}(z,\infty)$ is an increasing function of z for all k. For $\beta = 4$, Figure 2f shows that the CLD has become even more nonuniform, with distributions being more strongly peaked at small k near the rear of the layer than at the front. The maximum values of $w_{RM_kR}(z,\infty)$ (i.e., for $k = X_{max}(z,\infty)$) differ by more than a factor of 7 between the front and rear. These effects are clearly consequences of significant monomer conversion

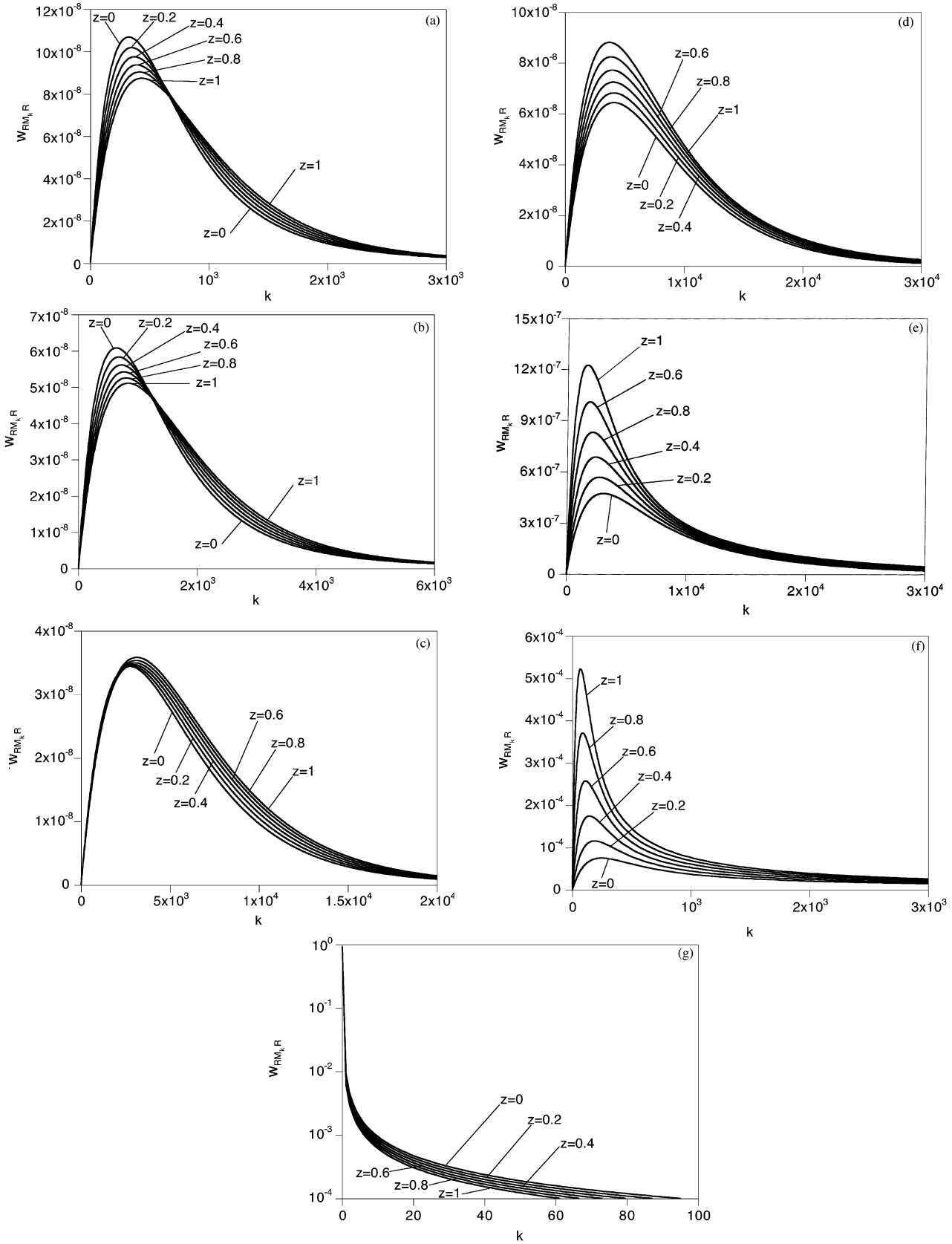

Figure 2. Final chain-length distribution at six uniformly spaced z-locations between the front ($z = 0$) and rear ($z = 1$) of the layer for $\gamma = 1$ and $\zeta = 10^{-4}$: (a) $\beta = 0.05$; (b) $\beta = 0.1$; (c) $\beta = 0.5$; (d) $\beta = 1$; (e) $\beta = 2$; (f) $\beta = 4$; (g) $\beta = 100$.

at low radical concentrations, long before most downbeam initiator has been consumed.

At the largest β (100), Figure 2g shows that monomer conversion is so complete prior to exhaustion of initiator that most primary radicals recombine with each other, leading to $X_{max} = 0$. (Note the logarithmic scale for the mole fractions.) A fully logarithmic plot over the range $1 \leq k \leq 10^5$ shows that mole fractions decrease nearly

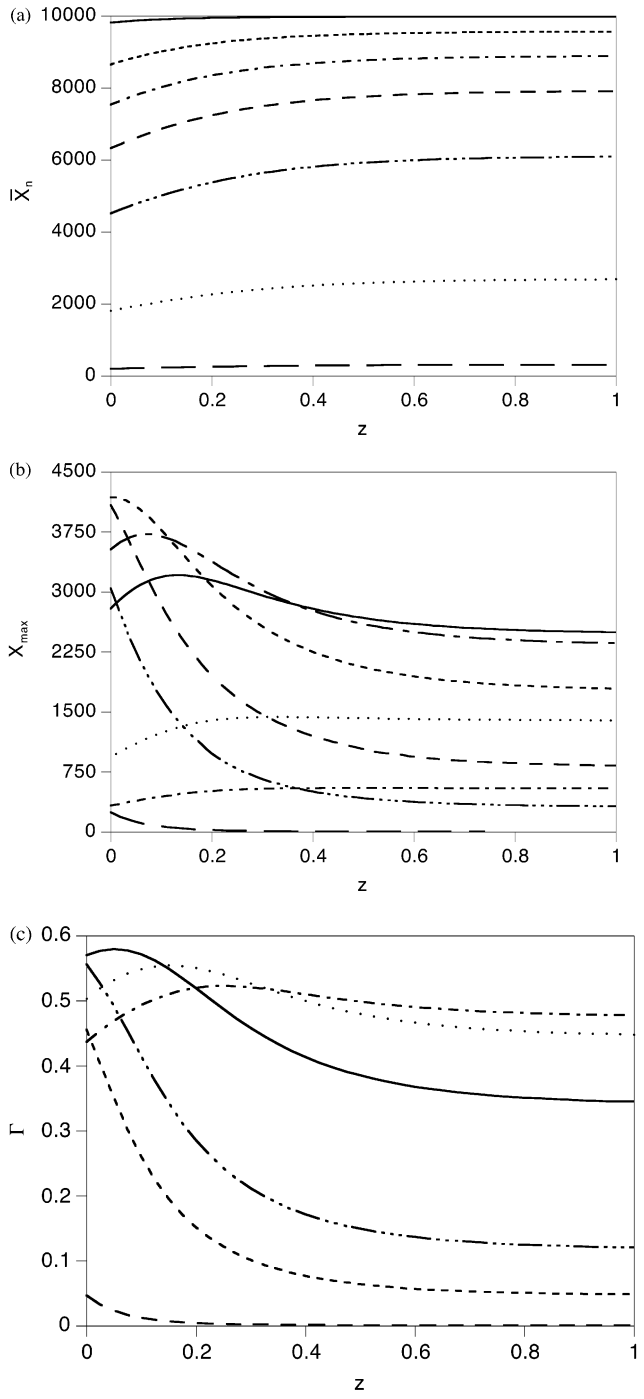

Figure 3. Spatial variation of $\overline{X}_n(z,\infty)$, $X_{max}(z,\infty)$, and $\Gamma(z)$ for $\gamma = 10$ and $\zeta = 10^{-4}$ for selected values of β. (a) $\overline{X}_n(z,\infty)$: (— —) $\beta = 0.01$; (···) $\beta = 0.1$; (— ··· —) $\beta = 0.3$; (— —) $\beta = 0.5$; (— · — · —) $\beta = 0.7$; (- -) $\beta = 1$; (——) $\beta = 2$. (b) $X_{max}(z,\infty)$: (— · — · —) $\beta = 0.05$; (···) $\beta = 0.15$; (——) $\beta = 0.5$; (— · —) $\beta = 0.7$; (- -) $\beta = 1$; (— —) $\beta = 1.5$; (— ··· —) $\beta = 2$; (—— ——) $\beta = 4$. (c) $\Gamma(z)$: (— · — · —) $\beta = 0.01$; (···) $\beta = 0.3$; (——) $\beta = 0.7$; (— ··· —) $\beta = 1.5$; (- -) $\beta = 2$; (— —) $\beta = 4$.

inversely with k at each z, with power-law fits to the k dependence over this range giving exponents of −1.002 at $z = 0$ and −1.083 at $z = 1$.

$\gamma = 10$. For $\gamma = 10$, Figure 3a shows that the plots of $\overline{X}_n(z,\infty)$ have considerably more curvature than for $\gamma = 1$, particularly for intermediate β. This is due to greater localization of absorbance and initiation near the front of the layer at higher γ, with the consequence of lower radical concentrations, and hence slower recombination, in a larger part of the remainder of the layer. Put differently, as γ increases, conversion of a significant fraction of monomer occurs under conditions of low radical concentration in a larger rear portion of the layer. For each β, we also note that the values of $\overline{X}_n(1,\infty)$ are greater than at $\gamma = 1$. (Values of $\overline{X}_n(0,\infty)$ are necessarily independent of γ.) Figure 3b shows that, at each β, variation of X_{max} with z is considerably greater than for $\gamma = 1$. These consequences are again due to greater degrees of nonuniformity in the initiation rate, monomer conversion rate, and radical concentrations as γ increases.

For $\gamma = 10$, Figure 3c shows that the maximum Γ is achieved at a smaller β (≈ 0.3) and Γ varies much more over the layer at each β, than for $\gamma = 1$. Unlike the results for $\gamma = 1$, there appears to be no β for which Γ increases monotonically with z. For $\gamma = 10$, the degree of polydispersity becomes increasingly nonuniform as β increases. However, the maximum value of Γ is nearly identical for $\gamma = 1$ and 10, and for each β, the polydispersity over most of the layer is *lower* at $\gamma = 10$ than at $\gamma = 1$. As shown below, the rapid decrease in Γ with z as β increases is due to the rapidly increasing fraction of downbeam monomer conversion that occurs at low radical concentrations. This leads to formation of a small number of long chains before significant initiator is consumed, and to a large number of short chains when initiator is consumed later.

The CLDs for $\gamma = 10$ are shown in Figure 4a−g. At the smallest β (0.05), Figure 4a shows that as z increases, X_{max} increases and w_{RM_kR} at X_{max} decreases, as for $\gamma = 1$ (Figure 2a). The CLDs broaden downbeam, with the half-width at half-maximum increasing from 423 at $z = 0$ to 688 at $z = 1$, and Γ increasing slightly from 0.44 to 0.48 from front to rear. Unlike the $\gamma = 1$ case, shifts in X_{max} at $\gamma = 10$ are no longer approximately linear in z, and spatial variation of CLDs is largely localized to the front of the layer. For $\beta = 0.05$ and 0.1, Figure 4a,b shows that the CLDs at $z = 0.4$, 0.6, 0.8, and 1 are nearly independent of z, corresponding to attainment of the large-z asymptote farther upbeam than for $\gamma = 1$. The $z = 0$ CLDs are necessarily independent of γ, while sufficiently far downbeam, comparison to results for $\gamma = 5$ (not shown) demonstrates that the CLD is nearly the same for $\gamma = 5$ and 10. At intermediate depths (e.g., $z = 0.2$), the maximum of the CLD is smaller for $\gamma = 10$ than for $\gamma = 5$, and occurs at a larger k. For small β, transition from the γ-independent CLD at $z = 0$ to the downbeam CLD occurs in a progressively smaller range of z as γ increases. For $\beta = 0.1$, Figure 4b shows that the CLD at each z is considerably broader than for $\beta = 0.05$ and decays less rapidly with increasing k.

For $\gamma = 10$ and $\beta = 0.5$, Figure 4c shows that at X_{max}, w_{RM_kR} *increases* as z increases, unlike the behavior for $\beta = 0.05$ and 0.1. The decrease in X_{max} with increasing z for $z \geq 0.2$ also differs from the behavior predicted for $\gamma = 1$, for which X_{max} increases with z. These results are evidently due to the fact that, as β increases, a larger fraction of the initial downbeam monomer is converted before significant local initiator is consumed, so that by the time significant incident light intensity reaches downbeam initiator, relatively little monomer remains. Thus, as β increases, an increasing fraction of downbeam initiation leads to relatively short chains. This trend becomes more pronounced for larger β, as shown in Figure 4d−f for $\beta = 1$, 2, and 4. As indicated by Figure

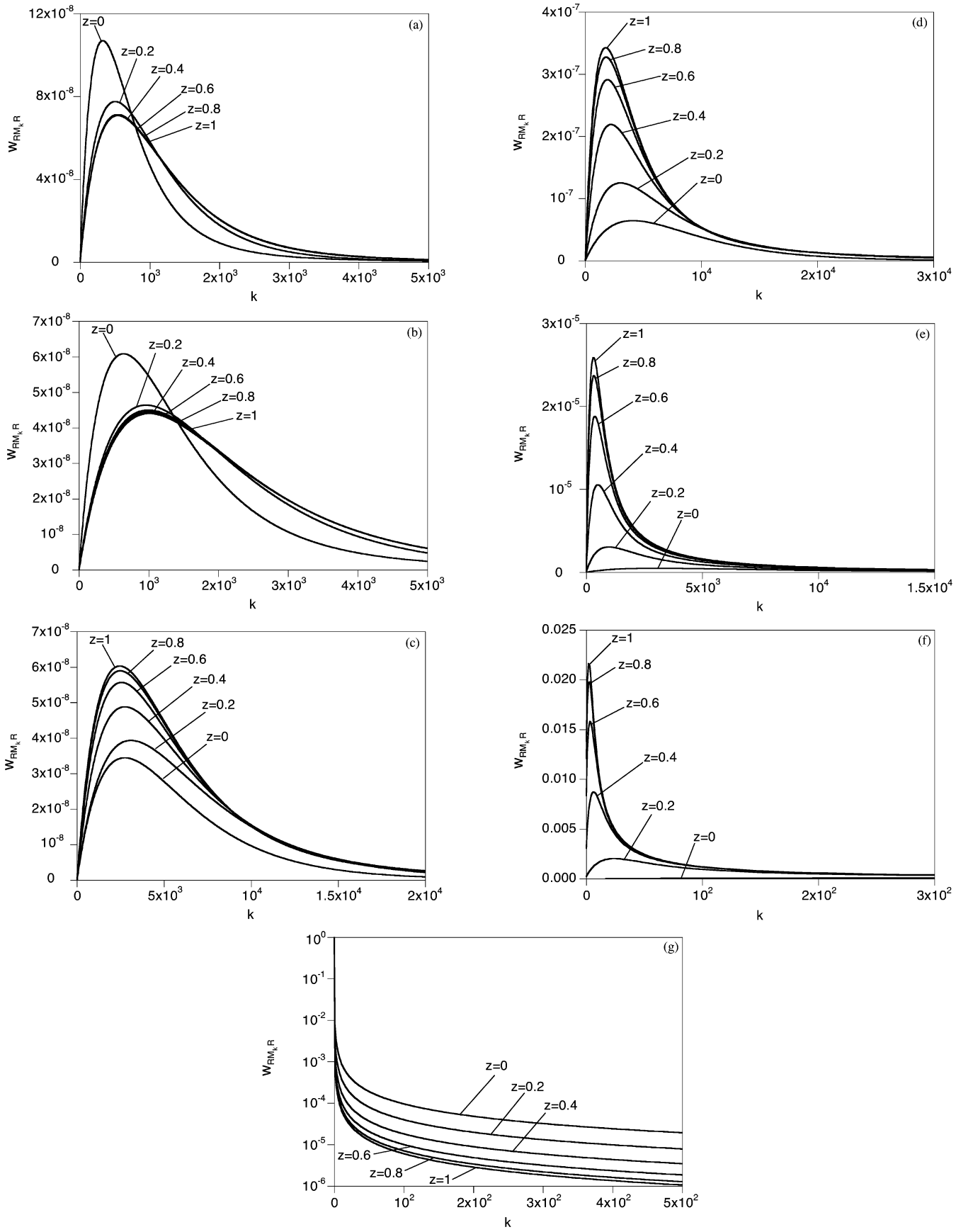

Figure 4. Final chain-length distribution at six uniformly spaced z-locations between the front ($z = 0$) and rear ($z = 1$) of the layer for $\gamma = 10$ and $\zeta = 10^{-4}$: (a) $\beta = 0.05$; (b) $\beta = 0.1$; (c) $\beta = 0.5$; (d) $\beta = 1$; (e) $\beta = 2$; (f) $\beta = 4$; (g) $\beta = 100$.

3b, for $\beta \geq 1$, X_{max} shifts to smaller k at each z. This considerable narrowing of the downbeam CLDs and movement of their maxima toward smaller k occurs after monomer conversion is essentially complete and

is a reflection of the fact that, as β increases, an increasing fraction of initiation *at each z* leads to small chains.

For $\beta = 0.5$ and 1, comparison of parts c and d of Figure 4 to results for $\gamma = 5$ shows that the CLDs at $z > 0$ now depend on γ, unlike the $\beta = 0.05$ and 0.1 cases. Thus, for these larger values of the kinetic parameter, downbeam CLDs depend on γ, β, and z. Note that for $\gamma = 10$ and $\beta = 1$, Figure 3c of ref 5 shows that at the end of reaction (i.e., when all initiator has been consumed), an essentially uniform 95% of initial monomer has been converted over $0.4 \leq z \leq 1$, and that farther upbeam, the converted monomer fraction gradually decreases to about 87% at $z = 0$. On the other hand, Figure 4d shows that at $z = 1$, the peak mole fraction w_{RM_kR} (at X) is more than 50% higher than at $z = 0.4$, and is more than a factor of 5 higher than at $z = 0$. These results show that the CLD can be much less uniform than the monomer conversion profile.

Figure 4e,f shows that, as β increases further, the $z > 0$ CLDs shift to smaller chain lengths and the mole fraction at $X_{max}(z,\infty)$ increases. For $\beta = 100$, Figure 4g shows, as for $\gamma = 1$, that the CLD falls off nearly inversely with k at each z. At each z, monomer conversion is so fast that essentially all initiator is consumed under conditions of very low monomer concentration, so that almost all primary radicals recombine with each other. As for $\gamma = 1$, $X_{max} = 0$ at each z. A logarithmic plot shows that the CLD again falls off nearly inversely with k for each z.

Thus, at each z, the maximum mole fraction (at X_{max}) initially decreases and then rapidly increases with increasing β. For example, at $z = 1$, the mole fractions at $X_{max}(1,\infty)$ are 6.4×10^{-8}, 4.3×10^{-8}, 6×10^{-8}, 3.4×10^{-7}, 2.6×10^{-5}, and 0.022 at $\beta = 0.05$, 0.1, 0.5, 1, 2, and 4, respectively. The rapid increase at larger β is a direct result of the strong β dependence of the rate of early downbeam monomer conversion at this high initial absorbance. As a result, by the time sufficient light has penetrated to consume downbeam initiator, most of the local monomer has been converted, leading to progressively more small chains. This is illustrated more clearly for $\gamma = 10$ than at smaller values of γ due to reduced downbeam optical penetration at larger γ.

Discussion

Mechanistic Sources of Nonuniformity. The results described above clearly demonstrate that nonuniform photoinitiation at nonzero values of the initial absorbance γ can give rise to CLDs with significant spatial nonuniformity. For a fixed value of $\zeta = C_{A,0}/C_{M,0}$, the final degree of nonuniformity depends on γ and dimensionless kinetic parameter β. More generally, nonuniformity of the final CLD will also depend on ζ.

Three related factors contribute to nonuniform CLDs. First, attenuation has the effect of spatially localizing initiation, to a degree that increases rapidly with γ.[2] Specifically, due to attenuation, initiator consumption is initially more rapid near the optical entrance ($z = 0$) than downbeam. In fact, initiator consumption at $z = \tau = 0$ is faster than at any other point at any other time. Second, as a consequence, initiator consumption near the optical entrance initially gives rise to, and occurs at, high concentrations of primary radicals and radical chains, resulting in higher rates of the termination reactions (4) than at any point downbeam or at any later time. The higher overall termination rate leads to a final mean chain length smaller at $z = 0$ than anywhere downbeam, as reflected in the monotonic increase of $\overline{X}_n(z,\infty)$ with z shown in Figures 1a and 3a. Third, for any γ, the fraction of downbeam monomer converted under conditions of very small radical concentration increases dramatically as β increases. The effect becomes more pronounced as γ increases, since at any sufficiently early time, the downbeam initiation rate and radical concentration both decrease monotonically as γ increases.

Within the limitations of our model, the results confirm our earlier conjecture[3] that the molecular weight distribution (or CLD) will vary from point to point, especially at high values of β and γ, in large part due to "beyond-the-front" polymerization at low radical concentrations.

Cessation of Illumination before Initiator Exhaustion. The final CLDs presented above correspond to those when all initiator has been consumed and monomer conversion ends. In fact, many photopolymerizations are stopped before exhaustion of initiator.[31,32] This is a particularly attractive strategy at large β, where monomer conversion can be essentially complete well before initiator is exhausted. Beyond reducing processing time, this approach will also reduce the large mole fractions of short chains predicted at high values of β (see especially Figures 2g and 4g), to an extent depending on when illumination ceases, as shown below.

For moderately large values of the initial absorbance ($\gamma = 10$) and kinetic parameter ($\beta = 100$), Figure 5a,b shows the temporal evolution of the CLDs at $z = 0$ and 1. When 90% of the monomer has been converted within the layer (at which time only 2.18% of the initiator in the layer has been consumed), $\overline{X}_n$ at $z = 0$ is 9.63×10^4. As reaction progresses, the CLD approaches the asymptotic form shown for $z = 0$ in Figure 4g, with the mole fraction decreasing essentially inversely with k. The values of $\overline{X}_n$ fall off with conversion, initially slowly to 8.84×10^4, 7.92×10^4, and 6.82×10^4 at monomer conversions of 91.41%, 93%, and 95%, respectively, and then rapidly to the asymptotic value of $\overline{X}_n \approx 10^4$ at 100% conversion (see (35)). The asymptotic mole fraction at each k is approached earlier as k increases. Figure 5b shows that the behavior at $z = 1$ is similar, but even more precipitous, with $\overline{X}_n$ shifting from 1.20×10^8 at 90% monomer conversion to 1.06×10^8, 7.98×10^7, and 4.17×10^7 at 95%, 99%, and 99.99% monomer conversion, respectively, before falling rapidly to $\overline{X}_n \approx 10^4$ at 100% conversion. Comparison of parts a and b of Figure 5 shows that for each overall fractional conversion considered, the CLD reaches its asymptotic form over a much wider range of k at $z = 1$ than at $z = 0$.

Implications for Experiment. The results presented above show that the final CLD can have much greater spatial nonuniformity than the degree of monomer conversion. For $\gamma = 1$ and $\beta = 4$, Figure 2f shows that $w_{RM_{246}R}(z,\infty)$ varies by a factor of 3.6 between $z = 0$ and 1, and that $w_{RM_{69}R}(z,\infty)$ varies by a factor of more than 11, where 246 and 69 are the chain lengths at which the final CLDs achieve their maxima at $z = 0$ and 1, respectively. The ratio $w_{RM_kR}(0,\infty)/w_{RM_kR}(1,\infty)$ can be larger or smaller than these values, depending on k. Comparison to the initiator (Figure 2b of ref 2) and monomer (Figure 6a) profiles shows that those quantities are much less nonuniform. On the other hand,

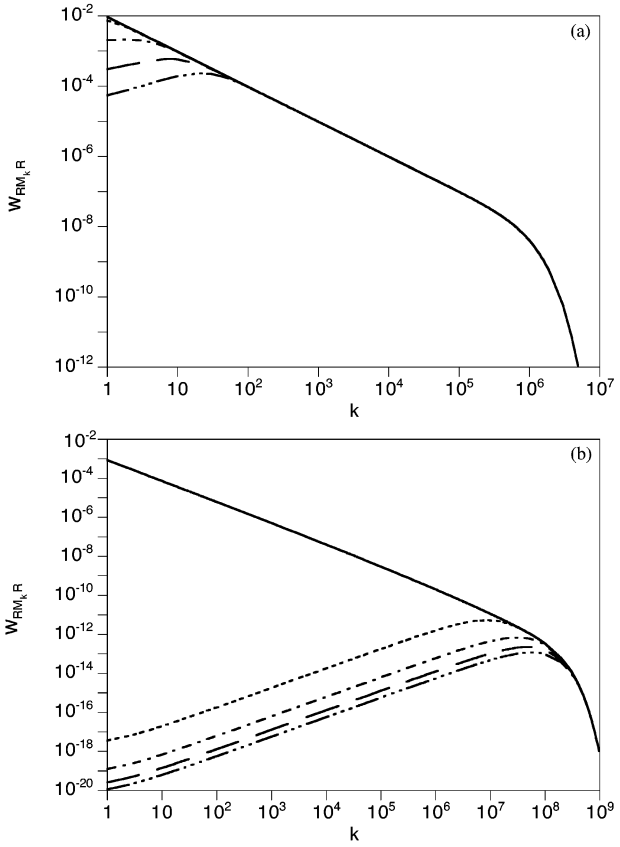

Figure 5. Temporal variation of the chain-length distributions for $\gamma = 10$ and $\beta = 100$ at $z = 0$ and 1 at different stages (indicated by parenthetical values of the layer-averaged fractional conversion of monomer and fractional consumption of initiator, respectively). (a) $z = 0$: (– ··· –) (0.90, 0.0688); (– –) (0.9141, 0.0766); (– · –) (0.9307, 0.0876); (- -) (0.95, 0.1044); (—) (1, 1). (b) $z = 1$: (– ··· –) (0.90, 0.0688); (– –) (0.95, 0.1044); (– · –) (0.99, 0.1810); (- -) (0.9999, 0.3313); (—) (1, 1).

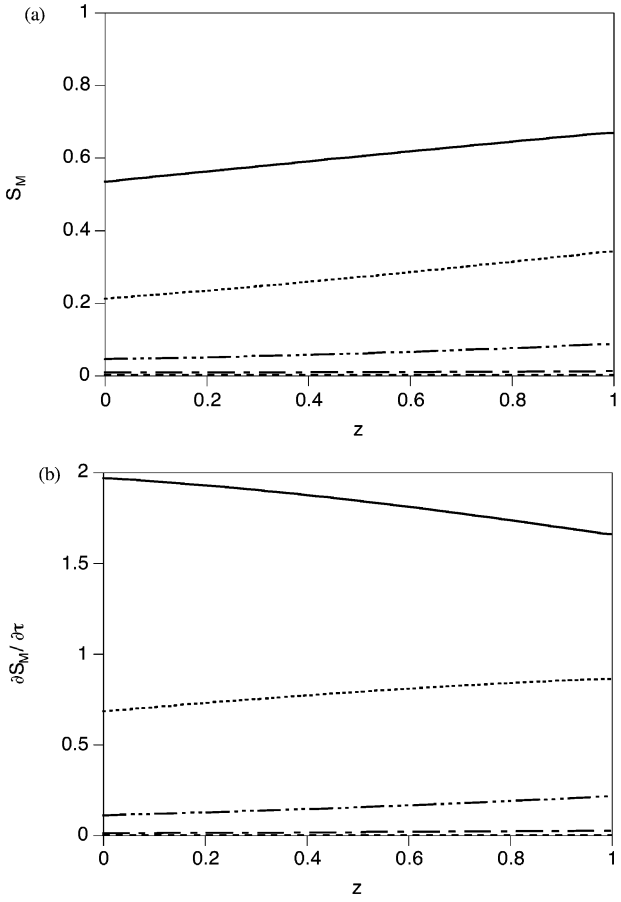

Figure 6. Spatiotemporal variation of dimensionless monomer concentration profiles and conversion rates as functions of $z = x/L$ for $\gamma = 1$, $\beta = 2$ at different fractional values of initiator consumption: (—) 0.9; (···) 0.75; (– ··· –) 0.5; (– · –) 0.25; (- -) 0.1. (a) $S_M = C_M/C_{M,0}$; (b) $-\partial S_M/\partial\tau$.

Figure 3b of ref 2 and Figure 6b show that the degrees of nonuniformity in the rates of initiator consumption and monomer conversion, respectively, are intermediate between the initiator and monomer concentration distributions on the one hand, and the final CLDs on the other.

These results demonstrate that CLD nonuniformity cannot be evaluated or predicted solely on the basis of the spatial variation of monomer conversion or photoinitiator consumption. If spatial variation of CLD-dependent properties in the photopolymerized material is of interest, our results strongly suggest that spatial variation of the CLD or its appropriate moments be directly measured.

Relationship to Previous Work. Absent previous work on spatial variation of CLDs, we confine our remarks here to the degree of CLD nonuniformity expected in previous free-radical photopolymerization experiments and simulations involving photobleaching initiators, in which nonuniform monomer conversion has been observed or predicted.

Mateo et al. investigated photopolymerization of methyl acrylate initiated by 4-(dimethylamino)-4′-isopropylbenzophenone, which photobleaches over most of the range of actinic wavelengths.[19] For the "unstirred" case (i.e., with no mass transfer), the initial absorbance that gives rise to the maximum initial layer-averaged photopolymerization rate in such a system has been estimated by Lissi and Zannoco[33] and Terrones and Pearlstein[3] to be $\gamma = 2.21$ and 2.51, respectively. For the values of β (~ 0.1) in the experiments of Mateo et al., the results in Figure 2a (for $\gamma = 1$) thus provide a lower bound on the degree of CLD nonuniformity, which is expected to be significant.

More recently, Goodner and Bowman[4] included attenuation and initiator consumption in a one-dimensional unsteady photopolymerization model incorporating a kinetic scheme with chain termination by recombination, and accounting for diffusion-limited propagation and termination at high monomer conversion. They considered 3 mm layers of 2-hydroxyethyl methacrylate at two concentrations of an initiator (2,2-dimethoxy-2-phenylacetophenone; DMPA) for which the absorbance of the layer is unchanged during reaction, and at one concentration of a hypothetical photobleaching initiator with the same absorption coefficient as DMPA. Contour plots of photopolymerization rate and one plot of fractional conversion of monomer showed clear evidence of nonuniformity at high initiation rates. If one neglects variation of propagation and termination rate "constants" at high conversion, the kinetic model can be accommodated by ours. For the photobleaching initiator case of interest here, the parameters used by Goodner and Bowman correspond to $\gamma = 22.5$ and $\beta = 28.8$. For this large initial absorbance and large kinetic parameter, our model predicts significant CLD nonuniformity over the front part of the layer, with computed values of the mole fractions decreasing monotonically with

increasing k at each z, and monotonically with z at each nonzero k. The variation is essentially confined to the front 40% of the layer, with the mole fractions at $z = 0$ exceeding those at $z = 0.4$ by factors increasing monotonically with k from 3.38 for $k = 0$ to 5.62 for $k = 100$.

Burdick, Peterson, and Anseth[20] recently reported spatially nonuniform monomer conversion in photopolymerization of methacrylated sebacic anhydride monomer initiated by benzoin ethyl ether (BEE) in layers 1 cm thick. To estimate the degree of CLD nonuniformity in their work, we again need values of γ and β. Using the extinction coefficient of BEE (780 M^{-1} cm^{-1})[34] at an unspecified (but apparently UV) wavelength, and the initiator concentration (0.1%) of Burdick et al., we get $\gamma = 7$. With regard to β, it appears that k_p and k_t in (15) have not been independently reported for this monomer. Hence, we use the approximate eq 4 of Burdick et al. to write

$$\frac{k_p}{k_t^{1/2}} = \left[\frac{-2}{R_{init}}\frac{d\bar{S}_M/dt}{\bar{S}_M}\right]^{1/2} \tag{37}$$

where R_{init} is the layer-averaged initiation rate. We then approximate the second factor in the bracket by a value of the ordinate shown in Figure 3 of the paper of Muggli et al.,[35] who measured the DMPA-initiated photopolymerization rate of the same monomer and reported results in terms of a quantity with the units of a first-order rate constant. In the cited figure, we chose the ordinate value of 0.01 s^{-1}, corresponding to the maximum value at the lowest DMPA concentration (0.1%) and the intensity closest to that used by Burdick et al. (The choice of the lowest DMPA concentration is motivated by the fact that high concentrations of nonbleaching initiators, such as DMPA, lead to significant "internal filtering" effects and lower layer-averaged polymerization rates than photobleaching initiators with comparable absorptivities and quantum yields.) Finally, we approximate the layer-averaged initiation rate using eq 23b of ref 2. We neglect the exponential term, which leads to negligible error for the large value of γ in ref 20. We take the quantum yield to be unity, set $f = 2$ (two radicals per initiator molecule photolyzed), and use $L = 2$ mm, giving $\beta = 0.6$. (Layer depths of 1, 2, and 3 mm were mentioned by Burdick et al., and since L appears as $L^{1/2}$, the choice made corresponds to an error of no more than 42% in β.) For $\gamma = 7$ and $\beta = 0.6$, computation shows that X_{max} varies nonmonotonically with z, between 2500 and 3500. The final mole fractions at $X_{max}(z,\infty)$ vary by more than a factor of 2, with the variation spread nearly uniformly over the layer, while for $k > 10^4$, the 2-fold variation in final mole fractions through the layer is essentially confined to the forward 20%.

Dependence on Ratio of Initiator and Monomer Concentrations. Like previous kinetic models of free-radical photopolymerization, our model[3] predicts that the fractional conversion of monomer at any position and time is independent of initial monomer concentration, $C_{M,0}$. As noted earlier,[3] this follows from the linear differential equation, eq 9, or from its dimensionless counterpart, eq 13, and is a property of the full set of equations, eq 5a−d.

On the other hand, as pointed out previously,[3] we expect that the CLD, and hence a number of physical properties, will depend on $C_{M,0}$. Since the rates of change of individual radical species concentrations ((5b) and (5c)) are not proportional to C_M, relative rates of constituent reactions of (5) will depend on $C_{M,0}$, as will ratios of radical concentrations. Thus, since the overall rates of termination reactions are proportional to products of pairs of radical concentrations, the CLD will shift to larger k as $C_{M,0}$ increases, if all else (including $C_{A,0}$) is held constant. In dimensionless terms, the CLD will shift to larger k as ζ increases.

Limitations of the Kinetic Model. Our model neglects dependence of the propagation and termination rate constants on the CLD, radical chain lengths, and degree of monomer conversion, which can be important in a number of systems.[36,37] The present model is nonetheless useful for at least three reasons. First, as pointed out by Russell,[38] chain-length dependent termination often leads to only small deviations from the predictions of "classical" (constant k_p and k_t) models. Second, even when chain-length dependent termination is significant, a constant k_p and k_t model against which comparison can be made is desirable. Finally, since dependence of these rate constants on the extent of reaction is due to reduced radical diffusion rates in the polymerizing medium, more detailed formulations will need to account for dependence of kinetics on the CLD rather than simply on the extent of monomer conversion or the lengths of diffusing radical chains, since widely different CLDs can correspond to exactly the same degree of monomer conversion. Thus, for each i in (3) and each combination of i and j in (4), the rate constants can be expected to depend on the *local* CLD of the medium through which recombining radicals diffuse. Such a model would go well beyond and be considerably more complex than standard treatments of "chain length dependent kinetics".[39,40] Development of a photopolymerization model predicting CLD nonuniformity lays the necessary groundwork for that.

Nonuniform temperature distributions due to heating by light absorption and exothermicity can significantly affect polymerization kinetics, through an Arrhenius-like temperature dependence of "elementary" rate constants, as well as through the viscosity of the medium in which radicals and monomer must diffuse to react. Thermal nonuniformity has been considered in simulations of monomer conversion.[5,41] Effects on CLDs are unexplored.

We have neglected diffusion in the species equations, (5), and assumed that all of the chemistry ensues from photolysis of a photobleaching initiator, absorbing at a single wavelength or with the same absorptivity over a range of wavelengths. Miller et al.[42] have presented a model accounting for effects of diffusion and wavelength-dependent absorption on initiator concentration distributions in photobleaching media. Effects on monomer conversion and CLDs are unknown. Diffusion of a given species should be unimportant when $D < L_{char}^2/t_{char}$, where D is the diffusion coefficient, and L_{char} and t_{char} are a characteristic length and time, respectively. If we take L_{char} and t_{char} to be the layer thickness and duration, respectively, then initiator diffusion in a low-viscosity solvent ($D \sim 10^{-6}$ cm^2 s^{-1}) will be unimportant in a 1 mm layer if the reaction time is less than 10^4 s, and in a 100 μm layer if less than 100 s. There are thus many systems for which $D < L_{char}^2/t_{char}$.

At high primary radical concentrations, primary radical recombination with either a primary radical or radical chain will be important, and the assumption of equal termination rate constants might lead to significant errors, as discussed previously.[37,43]

Finally, our model assumes that the local rates of initiator consumption and photon absorption are linear functions of the local light intensity (viz., eq 5a and the differential equation $\partial I/\partial x = -\alpha_A C_A I$ that gives rise to eq 6, respectively), and so is not appropriate for describing recently developed micro- and nanofabrication processes initiated by two-photon absorption.[17,18]

Conclusions

For free-radical photopolymerization with a photobleaching initiator and constant propagation and termination rate constants, we have shown how the final chain-length distribution in a layer depends on position over a range of the initial absorbance $\gamma = \alpha_A C_{A,0} L$ and on a second dimensionless kinetic parameter $\beta = k_p[fC_{A,0}/(\phi\alpha_A I_0 k_t)]^{1/2}$. The results show how the chain length distribution can be much more nonuniform than the fractional monomer conversion profile. The chain length distributions can be related to the spatiotemporal variation of initiation rate, with "downbeam" conversion of monomer at very low radical concentrations playing an important role. For several photopolymerization experiments described in the literature, considerable nonuniformity in the chain-length distribution can be expected.

Acknowledgment. Los Alamos National Laboratory is operated by the University of California for the U.S. Department of Energy under Contract W-7405-ENG-36.

References and Notes

(1) Flory, P. J. *Principles of Polymer Chemistry*; Cornell University Press: Ithaca, NY, 1953; p 114.
(2) Terrones, G.; Pearlstein, A. J. *Macromolecules* **2001**, *34*, 3195−3204.
(3) Terrones, G.; Pearlstein, A. J. *Macromolecules* **2001**, *34*, 8894−8906.
(4) Goodner, M. D.; Bowman, C. N. In *Solvent-Free Polymerizations and Processes. Minimization of Conventional Organic Solvents*; Long, T. E., Hunt, M. O., Eds.; ACS Symposium Series 713; American Chemical Society: Washington, DC, 1998; pp 220−231.
(5) Goodner, M. D.; Bowman, C. N. *Chem. Eng. Sci.* **2002**, *57*, 887−900.
(6) Lee, J. H.; Prud'homme, R. K.; Aksay, I. *J. Mater. Res.* **2001**, *16*, 3536−3544.
(7) Cook, W. D. *J. Dent. Res.* **1980**, *59*, 800−808.
(8) Cook, W. D. *J. Macromol. Sci.—Chem.* **1982**, *A17*, 99−111.
(9) Cook, W. D.; Standish, P. M. *Aust. Dent. J.* **1983**, *28*, 307−311.
(10) Hirose, T.; Wakasa, K.; Yamaki, M. *J. Mater. Sci.* **1990**, *25*, 1209−1213.
(11) Cook, W. D. *J. Appl. Polym. Sci.* **1991**, *42*, 2209−2222.
(12) Anseth, K. S.; Newman, S. M.; Bowman, C. N. In *Biopolymers II*; Peppas, N. A., Langer, R. S., Eds.; Advances in Polymer Science 122; Springer: New York, 1995; pp 177−217.
(13) Flach, L.; Chartoff, R. P. *Polym. Eng. Sci.* **1995**, *35*, 483−492.
(14) Flach, L.; Chartoff, R. P. *Polym. Eng. Sci.* **1995**, *35*, 493−498.
(15) Bertsch, A.; Jézéquel, J. Y.; André, J. C. *J. Photochem. Photobiol. A: Chem.* **1997**, *107*, 275−281.
(16) Recent exploitation[17,18] in micro- and nanofabrication applications of extremely localized photopolymerization initiated by two-photon absorption is based on a localization mechanism different from that considered here.
(17) Kawata, S.; Sun, H.-B.; Tanaka, T.; Takada, K. *Nature (London)* **2002**, *412*, 697−698.
(18) Tanaka, T.; Sun, H.-B.; Kawata, S. *Appl. Phys. Lett.* **2002**, *80*, 312−314.
(19) Mateo, J. L.; Bosch, P.; Vázquez, E.; Sastre, R. *Makromol. Chem.* **1988**, *189*, 1219−1227.
(20) Burdick, J. A.; Peterson, A. J.; Anseth, K. S. *Biomaterials* **2001**, *22*, 1779−1786.
(21) North, A. M. *The Kinetics of Free Radical Polymerization*; Pergamon: Oxford, England, 1966.
(22) Allcock, H. R.; Lampe, F. W. *Contemporary Polymer Chemistry*, 2nd ed.; Prentice Hall: Englewood Cliffs, NJ, 1990.
(23) Krongauz, V. V. In *Processes in Photoreactive Polymers*; Krongauz, V. V., Trifunac, A. D., Eds.; Chapman and Hall: New York, 1994; pp 185−259.
(24) Brulle, Y.; Bouchy, A.; Valance, B.; André, J. C. *J. Photochem. Photobiol. A: Chem.* **1994**, *83*, 29−37.
(25) Frazier, D. O.; Hung, R. J.; Paley, M. S.; Long, Y. T. *J. Cryst. Growth* **1997**, *173*, 172−181.
(26) We use the absorption coefficient (ref 27, p 21) for simplicity; it is related to the (decadic) molar absorptivity or extinction coefficient ϵ_A by $\alpha_A = \epsilon_A \ln 10$.
(27) Calvert, J. G.; Pitts, J. N. *Photochemistry*; Wiley: New York, 1966; pp 640−641.
(28) Decker, C. *Prog. Polym. Sci.* **1996**, *21*, 593−650.
(29) Decker, C.; Bendaikha, T.; Decker, D.; Zahouily, K. *Polym. Prepr.* **1997**, *38*, 487−488.
(30) Flory, P. J. *J. Am. Chem. Soc.* **1936**, *58*, 1877−1885.
(31) Hutt, A.; Ranby, B.; Yuan, Y. Y. *Polym. Degrad. Stab.* **1984**, *8*, 89−105.
(32) Hutt, A.; Yuan, Y. Y.; Ranby, B. *Polym. Degrad. Stab.* **1984**, *8*, 241−258.
(33) Lissi, E. A.; Zanocco, A. *J. Polym. Sci., Polym. Chem. Ed.* **1983**, *21*, 2197−2202.
(34) Woo, H.-G.; Hong, L.-Y.; Kim, S.-Y.; Choi, Y.-K.; Kook, S.-K.; Ham, H.-S. *Bull. Kor. Chem. Soc.* **1995**, *16*, 667−670.
(35) Muggli, D. S.; Burkoth, A. K.; Keyser, S. A.; Lee, H. R.; Anseth, K. S. *Macromolecules* **1998**, *31*, 4120−4125.
(36) Tryson, G. R.; Shultz, A. R. *J. Polym. Sci., Polym. Phys. Ed.* **1979**, *17*, 2059−2075.
(37) Goodner, M. D.; Bowman, C. N. *Macromolecules* **1999**, *32*, 6552−6559.
(38) Russell, G. T. *Aust. J. Chem.* **2002**, *55*, 399−414.
(39) Benson, S. W.; North, A. M. *J. Am. Chem. Soc.* **1962**, *84*, 935−940.
(40) Olaj, O. F.; Kornherr, A.: Vana, P.; Zoder, M.; Zifferer, G. *Macromol. Symp.* **2002**, *182*, 15−30.
(41) Lecamp, L.; Lebaudy, P.; Youssef, B.; Bunel, C. *Polymer* **2001**, *42*, 8541−8547.
(42) Miller, G. A.; Gou, L.; Narayanan, V.; Scranton, A. B. *J. Polym. Sci., Part A: Polym. Chem.* **2002**, *40*, 793−808.
(43) Bamford, C. H. *Trans. Faraday Soc.* **1959**, *55*, 1451−1460.

MA021589K